

On the contribution of Rossby waves driven by surface buoyancy fluxes to low-frequency North Atlantic steric sea surface height variations

Peter Kowalski*

Department of Physics, Imperial College, London, UK

Abstract

Previous studies have shown that wind-forced baroclinic Rossby waves can capture a large portion of low-frequency steric SSH variations in the North Atlantic. In this paper, we extend the classical wind-driven Rossby wave model derived in a 1.5 layer ocean to include surface buoyancy forcing, and then use it to assess the contribution from buoyancy-forced Rossby waves to low-frequency North Atlantic steric SSH variations. In the tropical-to-mid-latitude North Atlantic we find that wind-driven Rossby waves are dominant, however, in the eastern subpolar North Atlantic their contribution is roughly the same as that of buoyancy-forced Rossby waves, where together they capture up to 50% of low-frequency steric SSH variations.

Keywords: Sea surface height, Rossby waves, subpolar North Atlantic.

1. Introduction

In the North Atlantic variations in sea surface height (SSH) on interannual and longer timescales have been shown to be primarily due to variations in steric SSH (e.g. Forget and Ponte 2015; Polkova et al., 2015; Piecuch and Ponte 2011; Piecuch and Ponte 2012b, 2012a), which is defined as

$$\eta_S = -\frac{1}{\rho_0} \int_{-D}^0 \Delta\rho \, dz, \quad (1)$$

where η_S denotes the steric SSH, D is the ocean depth, and $\Delta\rho = \rho - \rho_0$ is the density anomaly with ρ_0 a characteristic ocean density. Many studies have thus linked low-frequency steric SSH variations in the North Atlantic to wind-forced baroclinic Rossby waves (e.g. Sturges et al. 1998; Cabanes et al. 2006; Zhang and Wu 2010; Polkova et al. 2015; Zhang et al. 2016; Calafat et al. 2018), which can take many years to cross an ocean basin and are therefore thought to influence climate on decadal timescales (e.g. Schneider and Miller

*Corresponding author

Email address: p.kowalski@imperial.ac.uk (Peter Kowalski)

2001). In particular, all previous studies combined have shown that the linear first baroclinic mode Rossby wave model forced by winds can capture a significant portion of both the phase and amplitude of steric SSH variations in the interior of the eastern North Atlantic, but that it is generally less skillful in the western part of the basin (e.g. Cabanes et al. 2006; Zhang and Wu 2010; Zhang et al. 2016). With regards to buoyancy-forced Rossby waves, Piecuch and Ponte [2012b] showed that they significantly influence the phase of the steric SSH in the tropical South Atlantic, however, their contribution to low-frequency North Atlantic steric SSH variations in the North Atlantic is yet to be explored.

The most widely used Rossby wave model of the steric SSH in the literature is the wind-driven Rossby wave model derived in a 1.5-layer ocean (e.g. Schneider and Miller, 2001; Zhang and Wu, 2010). In this framework the density is modelled as two layers of constant density with the interface between the two layers taken to represent the depth of the pycnocline, which is the depth in the permanent pycnocline at which the vertical density gradient is a local maximum (e.g. Feucher et al., 2016). Furthermore, the ocean dynamics are governed by the upper ocean linear vorticity balance in a wind-driven ocean that is in geostrophic and hydrostatic balance, but with only the layer above the pycnocline depth in motion. In this paper we allow the upper layer density in the classical 1.5 layer ocean model framework to vary and subsequently extend the wind-driven Rossby wave model to include surface buoyancy forcing.

This paper is organised as follows: In Section 2 we describe the (model) data set used in this study (the “observations”) and methodology. In Section 3 we examine the role of Rossby waves forced by surface buoyancy fluxes by comparing low-frequency SSH variations predicted by the wind-and buoyancy-forced Rossby wave model derived in a 1.5 layer ocean (e.g. Huang 2012) with those of the “observed”; The derivation of this model can be found in the appendix. Section 3 also includes a summary of the findings along with some suggestions for future work.

2. Data and methodology

The data set that we use is the ECCO v4r1 ocean state estimate (Forget et al., 2016) produced by the Estimating the Circulation and Climate of the Ocean (ECCO) consortium (Wunsch and Heimbach, 2007). The data covers the period 1992-2011. Furthermore, the horizontal resolution of this particular solution in the North Atlantic is 0.25° with 50 vertical levels of varying thickness, and the time resolution is monthly. For a detailed description of the ECCO v4r1 ocean state estimate see Liang et al. [2017], who used this version of the solution to study bi-decadal changes in ocean heat content. Data for all the relevant variables (e.g. surface

heat fluxes, density and wind-stress) used in this study are readily available in ECCO v4r1.

The model steric SSH, denoted by η_ρ , is computed using Eq. (1) with $\rho_0 = 1027\text{kgm}^{-3}$. We form time series of anomalies for η_ρ , and the forcing terms in the Rossby wave model, by removing the time mean, linear trend and seasonal cycle. The resulting time series of anomalies for the forcing terms are then used to derive time series of model-simulated steric SSH anomalies, which are denoted by η_S . The time series of η_S and η_ρ are then low-pass filtered to remove any signals shorter than 1 year to focus on interannual-to-decadal timescales. The time series η_S that are the best match to η_ρ are determined from the skill metric

$$S = \left(1 - \frac{\langle (\eta_\rho - \eta_S)^2 \rangle}{\langle \eta_\rho^2 \rangle}\right) \times 100\%. \quad (2)$$

In this formula values of S range from $-\infty$ to 100%. $S \rightarrow 100\%$ indicates that η_S is very close to η_ρ in both phase and amplitude while $S < 0$ indicates that η_S may capture the phase but overestimates the magnitude of η_ρ . Briefly, we found that the regions with statistically significant predictions of η_ρ are roughly those with $S > 10\%$, therefore, in all figures showing forecast skill [Fig. 2] the regions in which $S < 10\%$ have been masked.

3. Response of steric SSH to buoyancy-forced Rossby waves

As shown in the appendix, in a simple 2-layer geostrophic and hydrostatic ocean with upper layer density that varies with space and time, the steric SSH can be written

$$\eta_S = \eta_P + \eta_L, \quad (3)$$

where η_L is the component of η_S that is associated with local surface buoyancy fluxes and η_P is associated with wind- and buoyancy-forced baroclinic Rossby waves. In this section we focus on the contribution of η_P to η_S . The Rossby wave equation for η_P is

$$\frac{\partial \eta_P}{\partial t} + C_R \frac{\partial \eta_P}{\partial x} = -\frac{g'}{g} W_E - \frac{B}{2\rho_0} - \epsilon \eta_S, \quad (4)$$

where t, x, y refer to time and the distances in the east-west and north-south directions, respectively, g' is the reduced gravity, C_R is the Rossby wave phase speed, W_E is the local Ekman pumping that is derived using the wind-stress $\boldsymbol{\tau}$ from ECCO v4r1, B is a source of buoyancy, and note that we have added dissipation ϵ which represents, among other possible mechanisms, destabilization of long Rossby waves by baroclinic instability (Lacasce and Pedlosky 2004). Following Piecuch and Ponte [2012b] we assume that B represents mixed layer

fluxes of heat and freshwater, however, as in Cabanes et al. [2006], we find that freshwater fluxes are negligible over the entire North Atlantic (not shown), therefore,

$$-\frac{B}{\rho_0} = \frac{\alpha_T Q_{net}}{\rho_0 c_p}, \quad (5)$$

where Q_{net} is the surface heat flux in ECCO v4r1, $\alpha_T = 2 \times 10^{-4} \text{K}^{-1}$ is the coefficient of thermal expansion and $c_p = 4028 \text{JKg}^{-1} \text{K}^{-1}$ is the specific heat capacity.

The analytical solution to Eq. (4) is obtained by integrating along Rossby wave characteristics $x - C_R t = \text{constant}$ (e.g. Cabanes et al., 2006; Fu and Qiu, 2002). The resulting solution after replacing $-B/\rho_0$ with Eq. (5) is

$$\eta_P = \eta_B + F_{W_E} + F_Q, \quad (6)$$

where

$$\eta_B = \exp\left(\epsilon \frac{x_E - x}{C_R}\right) \eta_S\left(x_E, y, t + \frac{x_E - x}{C_R}\right), \quad (7)$$

$$\begin{aligned} F_{W_E} &= -\frac{g'}{g C_R} \int_{x_E}^x W_E\left(x', y, t + \frac{x' - x}{C_R}\right) \\ &\times \exp\left(\epsilon \frac{x' - x}{C_R}\right) dx', \end{aligned} \quad (8)$$

$$\begin{aligned} F_B &= \frac{\alpha_T}{2\rho_0 c_p C_R} \int_{x_E}^x Q_{net}\left(x', y, t + \frac{x' - x}{C_R}\right) \\ &\times \exp\left(\epsilon \frac{x' - x}{C_R}\right) dx', \end{aligned} \quad (9)$$

and $\eta_S(x_E, y, t)$ is the eastern boundary steric SSH, which is computed using the ECCO model proxy for the observed steric SSH, η_ρ , [see Section. 2] at the eastern boundary, x_E . As seen in Fig. 2, the eastern is a few degrees away from the coastlines and note that it is similar to that of Zhang et al. [2016]. Briefly, we performed model simulations in which we varied the position of the eastern boundary and found that moving it closer to the coastlines reduces the skill of the model in the interior of the eastern North Atlantic (not shown). The reduction in skill could be due to the inclusion of SSH anomalies that are associated with other factors instead of westward propagating baroclinic Rossby waves (e.g. topography or coastally trapped waves, as suggested by Zhang et al. 2016).

We assess the contribution of buoyancy-forced Rossby waves by comparing forecast skill [Eq. (2)] derived when $F_Q \neq 0$ and $F_Q = 0$ in Eq. (6). Following previous studies (e.g. Zhang and Wu 2010; Zhang et al. 2016), we let g' , ϵ and C_R depend on latitude for simplicity. Estimates for these parameters are derived by finding g' , ϵ and C_R that yield the largest values for forecast skill when $F_Q \neq 0$ and $F_Q = 0$ at each grid

point, and then finding the zonal average for each parameter over both experiments but only using the regions where the forecast skill is greater than 10%. In these experiments we let $g' \in [0.01\text{ms}^{-2} \sim 0.06\text{ms}^{-2}]$ and $\epsilon \in [(0.01\text{yr})^{-1} \sim (16\text{yr})^{-1}]$ (e.g. Zhang and Wu 2010; Zhang et al. 2016), and for C_R we first obtain an estimate at each latitude using the Lioville-Green approximation (e.g. Piecuch and Ponte 2012b),

$$C_R = \frac{\beta}{\pi f^2} \left[\left\langle \int_{-D}^0 N(x, y, z) \right\rangle \right]^2, \quad (10)$$

and then allow C_R to vary around this estimate. In the above equation, $\beta = df/dy$, N is the Brunt-Vaisala frequency computed at each grid point using the time-mean density in ECCO v4r1, and $\langle . \rangle$ denotes zonal average at each latitude. Fig. 1 shows g' [Fig. 1(a)], ϵ [Fig. 1(b)] and C_R [Fig. 1(c)]. Note that g' , which is a measure of the ocean stratification, decreases roughly monotonically from the tropics to the poles; ϵ in the tropics is much larger than in the subtropical-to-subpolar North Atlantic; and C_R is very similar to that obtained by Zhang & Wu [2010] and Zhang et al. [2016]. Note further that the values for forecast skill derived by finding optimal g' , ϵ and C_R at each grid point are similar to those that are obtained using the parameter values in Fig. 1 (not shown). Finally, similar to Chelton and Schlax [1996], we find that there is a discrepancy between C_R in Fig. 1(c), which is the phase speed of our observed proxy for the steric SSH, and that predicted by Eq. (10). In the literature this difference has been linked to factors such as inclusion of relative vorticity and Doppler shift by the depth mean flow (e.g. Tulloch et al. 2009; Samelson, 2010; Klocker and Marshall, 2014), effects which are absent in Eq. (10) and our Rossby wave model.

3.1. Results and discussion

Fig. 2(a) shows the forecast skill S_1 when the solution for η_P in Eq. (6) is determined when $F_Q = 0$ and Fig. 2(b) shows forecast skill S_2 when $F_Q \neq 0$. As in Cabanes et al. [2006], the effect of eastern boundary steric SSH anomalies, which in our model can be determined by isolating η_B in Eq. (6), is confined to the regions near the eastern boundary, and although we do not show figures for this result, this effect of η_B can be easily deduced from both Fig. 2(a) and Fig. 2(b). The regions where S_1 and S_2 are greater than 10% are generally the same with the exception of some parts of the subtropical North Atlantic. In the interior tropical-to-mid-latitude North Atlantic, it can be seen that the difference between S_2 and S_1 is relatively small, which shows that wind-forced Rossby waves dominate in this region. In the eastern subpolar North Atlantic from $55 - 60^\circ\text{N}$, S_1 and S_2 range from 20-30% and 40-50% respectively, therefore, the contribution of buoyancy-forced Rossby waves is roughly the same as that of wind-driven Rossby waves. However, note that in the western subpolar North Atlantic from $50 - 55^\circ\text{N}$, it can be seen by comparing S_1 with S_2 that the inclusion of surface buoyancy forcing in Eq. (6) has led to a small reduction in forecast skill.

Previous studies (e.g. Cabanes et al. 2006; Zhang & Wu, 2010; Zhang et al. 2016) have found that wind-driven Rossby waves cannot be used to predict steric SSH variations in the Mid-Atlantic Ridge and the western subpolar North Atlantic, specifically the Labrador Sea. We obtain the same result [Fig. 2(a)] and as seen in Fig. 2(b), buoyancy-forced Rossby waves do not enhance the predictive skill of Eq. (6) in these regions of the North Atlantic. In the literature low-frequency steric SSH variations in these regions of the North Atlantic have been linked to other factors and processes instead of baroclinic Rossby waves. In particular, Buckley et al. [2014] showed that variations in upper ocean heat content, which was shown by Forget and Ponte [2015] to significantly influence the steric SSH across the entire North Atlantic, can be attributed to surface heat fluxes and Ekman transport, with bolus transports and diffusion also playing a key role in the subpolar North Atlantic. In addition, Osychny and Cornillion [2004] showed that the Mid-Atlantic Ridge breaks the coherent structure of baroclinic Rossby waves originating on the eastern side of the subtropical North Atlantic. Finally, note that buoyancy forcing enters the Rossby wave model via a local model for the upper ocean density content [Eq. (A.10) in the appendix] and extending this model to include some of the aforementioned factors may subsequently improve the predictive skill of the Rossby wave model.

Briefly, with regards to previous studies that have investigated the role of wind-driven Rossby waves in North Atlantic steric SSH variability, our results [Fig. 2(a)] are most similar to those obtained by Zhang et al. [2016], who also included damping in their wind-driven Rossby wave model, however, our values for forecast skill on the western side of the tropical-to-mid-latitude North Atlantic are generally higher. This difference may be partly due to the different data set used; Zhang et al. [2016] compare their model-simulated SSH with SSH from satellite altimetry, whereas we compared ours with a model steric SSH derived using data from the ECCOv4 ocean state estimate and is therefore not a pure observation.

Finally, there are many studies (e.g. Schneider and Miller, 2001; Capotondi and Alexander, 2001; Fu and Qiu, 2002) that suggest wind-driven Rossby waves play a role in the low-frequency variability of the steric SSH in the North Pacific, but the role of buoyancy forced Rossby waves is yet to be explored. It would thus be interesting to conduct a similar study for the North Pacific.

Acknowledgements

The author is grateful to Arnaud Czaja for constructive comments on an earlier version of the manuscript.

Appendix A. Linear oceanic model

Appendix A.1. Model framework

We consider a two-layer rectangular basin of constant depth, D , and linear perturbations about a reference state of rest. The free surface is $\eta_S(x, y, t)$ and the depth of the interface is $-H_1 + \eta_1$, where $-H_1$ is the depth of the interface at rest and $\eta_1(x, y, t)$ is the interface depth displacement. The upper layer density is $\rho_1(x, y, t)$ and for simplicity, we take the lower layer density to be constant, i.e. $\rho_2 = \hat{\rho}_2$. Under the assumption of geostrophy and hydrostatic balance the pressure, horizontal velocity field and linear vorticity balance in the upper layer are, respectively,

$$P_1 = -g\rho_1(z - \eta_S) \quad (\text{A.1})$$

$$\mathbf{u}_1 = \left(\frac{1}{f\rho_0}\right)(\hat{\mathbf{z}} \times \nabla_H P_1), \quad (\text{A.2})$$

$$\frac{\beta}{f} \int_{-H_1+\eta_1}^{-\delta_E} v_1 dz = W_E - \frac{\partial \eta_1}{\partial t}, \quad (\text{A.3})$$

and in the lower layer

$$P_2 = -\hat{\rho}_2 g(z + H_1 - \eta_1) - g\rho_1(-H_1 + \eta_1 - \eta_S), \quad (\text{A.4})$$

$$\mathbf{u}_2 = \frac{1}{f\rho_0}(\hat{\mathbf{z}} \times \nabla_H P_2), \quad (\text{A.5})$$

where g is gravity; ρ_0 a characteristic ocean density; δ_E is the Ekman layer; f the Coriolis parameter with β its meridional derivative; and $W_E = \hat{\mathbf{z}} \cdot (\nabla_H \times [\boldsymbol{\tau}/\rho_0 f])$ is the local Ekman pumping with $\boldsymbol{\tau}$ the wind-stress.

The upper layer density is decomposed as $\rho_1 = \hat{\rho}_1 + \rho'_1$ where the hat variable refers to the reference state and the prime a small deviation from it ($\rho'_1 \ll \hat{\rho}_1$). Combining Eq. (A.1-A.3), and then using this decomposition for ρ_1 and the standard approximations (e.g. $\eta_1/H_1 \ll 1$, $\rho_1/\rho_0 \approx 1$ and thin Ekman layer) yields the linearized upper layer linear vorticity balance,

$$\left(\frac{\beta g H_1}{f^2}\right) \frac{\partial \eta_S}{\partial x} + \left(\frac{H_1^2 \beta g}{2f^2 \rho_0}\right) \frac{\partial \rho'_1}{\partial x} = W_E - \frac{\partial \eta_1}{\partial t}. \quad (\text{A.6})$$

Similarly, Eq. (A.4) can be combined with Eq. (A.5) giving the following expression for the lower layer horizontal velocity field:

$$\mathbf{u}_2 = \left(\frac{g'}{f}\right)(\hat{\mathbf{z}} \times \nabla_H \eta_1) + \left(\frac{g}{f}\right)(\hat{\mathbf{z}} \times \nabla_H \eta_S) + \left(\frac{g H_1}{f \rho_0}\right)(\hat{\mathbf{z}} \times \nabla_H \rho'_1), \quad (\text{A.7})$$

where $g' = g(\hat{\rho}_2 - \hat{\rho}_1)/\rho_0$ is the reduced gravity. As in the classical 1.5 layer ocean we assume that the lower layer is at rest ($u_2 = 0$), which leads to the following relation for η_S :

$$\eta_S = -\frac{g'}{g}\eta_1 - \frac{H_1}{\rho_0}\rho'_1. \quad (\text{A.8})$$

Note that it can easily be shown using Eq. (1) that in our model framework η_S is the steric SSH. The time derivative of η_S is

$$\frac{\partial \eta_S}{\partial t} = -\frac{g'}{g} \frac{\partial \eta_1}{\partial t} - \frac{H_1}{\rho_0} \frac{\partial \rho'_1}{\partial t}. \quad (\text{A.9})$$

Now, since the reference state is at rest, there are no background horizontal density gradients that can generate upper layer density anomalies (ρ'_1) and the only physical mechanism left to do so is a surface buoyancy flux, B . Therefore,

$$\frac{\partial(H_1 \rho'_1)}{\partial t} = B, \quad (\text{A.10})$$

where $H_1 \rho'_1$ is the upper ocean density content, and then substituting this equation into Eq. (A.9) gives

$$\frac{\partial \eta_S}{\partial t} = -\frac{g'}{g} \frac{\partial \eta_1}{\partial t} - \frac{B}{\rho_0}. \quad (\text{A.11})$$

We show next that η_S can be written as the sum of a local component due to local surface buoyancy forcing, and a dynamical component that is associated with wind- and buoyancy-forced Rossby waves.

Appendix A.2. Local and Rossby wave steric SSH dynamics

The key step is to write the upper layer linear vorticity balance [Eq. (A.6)] as

$$\left(\frac{\beta g H_1}{f^2} \right) \frac{\partial \eta_P}{\partial x} = W_E - \frac{\partial \eta_1}{\partial t}, \quad (\text{A.12})$$

where

$$\eta_P = \eta_S + \frac{H_1}{2\rho_0} \rho'_1 \quad (\text{A.13})$$

is a sea surface height, and the subscript P here is for pressure since η_P arises from the vertically integrated meridional velocity [l.h.s of Eq. (A.3)]. Differentiating this equation and using Eq. (A.10) gives

$$\frac{\partial \eta_P}{\partial t} = \frac{\partial \eta_S}{\partial t} + \frac{B}{2\rho_0}. \quad (\text{A.14})$$

Substituting Eq. (A.11) into the above equation gives

$$\frac{\partial \eta_P}{\partial t} = -\frac{g'}{g} \frac{\partial \eta_1}{\partial t} - \frac{B}{2\rho_0}, \quad (\text{A.15})$$

and then combining this equation with Eq. (A.12) leads to the following wind- and buoyancy-forced Rossby wave equation for η_P :

$$\frac{\partial \eta_P}{\partial t} + C_R \frac{\partial \eta_P}{\partial x} = -\frac{1}{2\rho_0} B - \frac{g'}{g} W_E, \quad (\text{A.16})$$

where

$$C_R = -\frac{\beta g' H_1}{f^2} < 0, \quad (\text{A.17})$$

is the Rossby wave phase speed. The equivalent version of this equation in a continuously stratified ocean was derived by Piecuch & Ponte [2012b] using normal modes decomposition.

From Eq. (A.14) it follows that

$$\eta_S = \eta_P + \eta_L, \quad (\text{A.18})$$

where η_L is determined from

$$\frac{\partial \eta_L}{\partial t} = -\frac{B}{2\rho_0}, \quad (\text{A.19})$$

and is therefore the component of η_S that is associated with local surface buoyancy forcing. Note also that from Eq. (A.15) the interface depth displacement η_1 can also be similarly written as

$$\eta_1 = \frac{g}{g'}(-\eta_P + \eta_L). \quad (\text{A.20})$$

Finally, it is straightforward to see that when $B = 0$, Eq. (A.14-A.16) reduce to the following set of equations:

$$\eta_S = \eta_P, \quad (\text{A.21})$$

$$\eta_1 = -\frac{g}{g'}\eta_P, \quad (\text{A.22})$$

$$\frac{\partial \eta_P}{\partial t} + C_R \frac{\partial \eta_P}{\partial x} = -\frac{g'}{g}W_E. \quad (\text{A.23})$$

These equations are equivalent to those derived in the classical 1.5-layer ocean configuration.

References

- [1] Buckley, M.W., Ponte, R.M., Forget, G., Heimbach, P. 2014. Low-frequency SST and upper-ocean heat content variability in the North Atlantic. *J. Climate*. 27, 4996–5018.
- [2] Cababnes, C., Huck, T., Colin de Verdiere, A. 2006. Contributions of wind forcing and surface heating to interannual sea level variations in the Atlantic Ocean. *J. Phys. Oceanogr.* 36, 1739–1750.
- [3] Calafat, F.M., Wahl, T., Lindsten, F., Williams, J., Frajka-Williams, E. 2018. Coherent modulation of the sea-level annual cycle in the United States by Atlantic Rossby waves. *Nat. Commun.* 9 (1). DOI: 10.1038/s41467-018-04898-y.
- [4] Capotondi, A., Alexander, M.A. 2001. Rossby waves in the tropical North Pacific and their role in decadal thermocline variability. *J. Phys. Oceanogr.* 31, 3496–3515.
- [5] Chelton, D.B., Schlax, M.G. 1996. Global observations of oceanic rossby waves. *Science*. 272, 234–238.

- [6] Feucher, C., Maze, G., Mercier, H. 2016. Mean Structure of the North Atlantic Subtropical Permanent Pycnocline from In Situ Observations. *J. Atmospheric Ocean. Technol.* 33, 1285–1308. DOI: 10.1175/JTECH-D-15-0192.1.
- [7] Forget, G., Campin, J-M., Heimbach, P., Hill, C.N., Ponte, R.M., Wunsch, C. 2016. ECCO version 4: Second Release, <http://hdl.handle.net/1721.1/102062>.
- [8] Forget, G., Ponte, R.M. 2015. The partition of regional sea level variability. *Prog Oceanogr.* 137, Part A, 173–195.
- [9] Fu, L.L., Qiu, B. 2002. Low-frequency variability of the North Pacific Ocean: The roles of boundary- and wind-driven Rossby waves. *J. Geophys. Res.* 107, 3220. DOI:10.1029/2001JC001131.
- [10] Huang, R.X. 2012. Ocean Circulation: Wind-Driven and Thermohaline Processes. *Cambridge University Press*. <https://doi.org/10.1017/CBO9780511812293>.
- [11] Klocker, A., Marshall, D.P. 2014. Advection of eddies by depth-mean flow. *Geophys. Res. Lett.* 41, 3517–3521.
- [12] Lacasce, J.H., Pedlosky, J. 2004. The instability of Rossby basin modes and the oceanic eddy field. *J. Phys. Oceanogr.* 34, 2027–2041.
- [13] Liang, X., Piecuch, C.G., Ponte, R.M., Forget, G., Wunsch, C., Heimbach, P. 2017. Change of the Global Ocean Vertical Heat Transport over 1993-2010. *J. Climate.* 30(14), 5319–5327.
- [14] Osychny, V., Cornillon, P. 2004. Properties of Rossby Waves in the North Atlantic Estimated from Satellite Data. *J. Phys. Oceanogr.* 34, 61–76.
- [15] Piecuch, C. G., Ponte, R.M. 2011. Mechanisms of interannual steric sea level variability. *Geophys. Res. Lett.* 38, L15605. DOI:10.1029/2011GL048440.
- [16] Piecuch, C. G., Ponte, R.M. 2012a. Buoyancy-driven interannual sea level changes in the southeast tropical Pacific. *Geophys. Res. Lett.* 39. <https://doi.org/10.1029/2012GL051130>.
- [17] Piecuch, C. G., Ponte, R.M. 2012b. Buoyancy-Driven Interannual Sea Level Changes in the Tropical South Atlantic. *J. Phys. Oceanogr.* 43, 533–547.
- [18] Polkova, I., Köhl, A., Stammer, D. 2015. Predictive skill for regional interannual steric sea level and mechanisms for predictability. *J. Climate.* 28, 7407–7419. DOI:10.1175/JCLI-D-14-00811.1.

- [19] Samelson, R.M. 2010. An effective-beta vector for linear planetary waves on a weak mean flow. *Ocean Modell.* 32, 170–174.
- [20] Schneider, N., Miller, A. J. 2001. Predicting western North Pacific Ocean climate. *J. Climate.* 14, 3997–4002.
- [21] Sturges, W., Hong, B., Clarke, A.J. 1998. Decadal wind forcing of the North Atlantic subtropical gyre. *J. Phys. Oceanogr.* 28, 659–668. DOI:10.1175/1520-0485(1998)028,0659:DWFOTN.2.0.CO;2.
- [22] Tulloch, R., Marshall, J., Smith, K.S. 2009. Interpretation of the propagation of surface altimetric observations in terms of planetary waves and geostrophic turbulence. *J. Geophys. Res.* 114, C02005, doi: 10.1029/2008JC005055.
- [23] Wunsch, C., Heimbach, P. 2007. Practical global oceanic state estimate. *Physica D.* 230, 197–208.
- [24] Zhang, J., Kelly, K.A., Thompson, L.A. 2016. The role of heating, winds, and topography on sea level changes in the North Atlantic. *J. Geophys. Res. Oceans.* 121, 2887–2900. DOI:10.1002/2015JC011492.
- [25] Zhang, H., Wu, L. 2010. Predicting North Atlantic sea surface temperature variability on the basis of the first-mode baroclinic Rossby wave model. *J. Geophys. Res.* 115. C09030. DOI: 10.1029/2009JC006017.

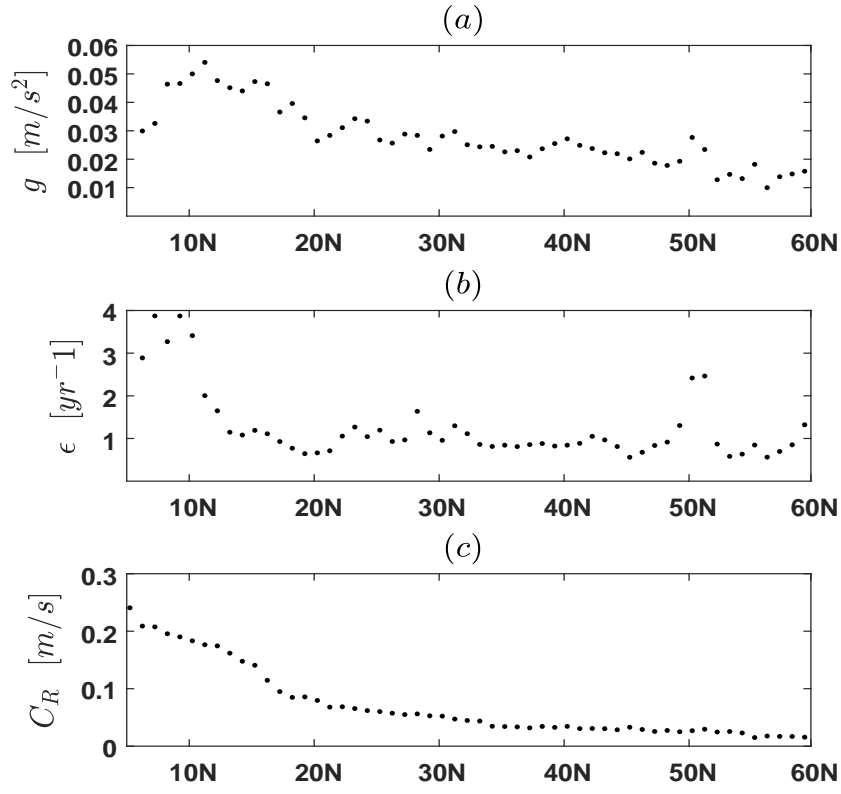


Fig. 1: (a) shows reduced gravity, g' , (b) is the dissipation rate, ϵ , and (c) is the Rossby wave phase speed C_R

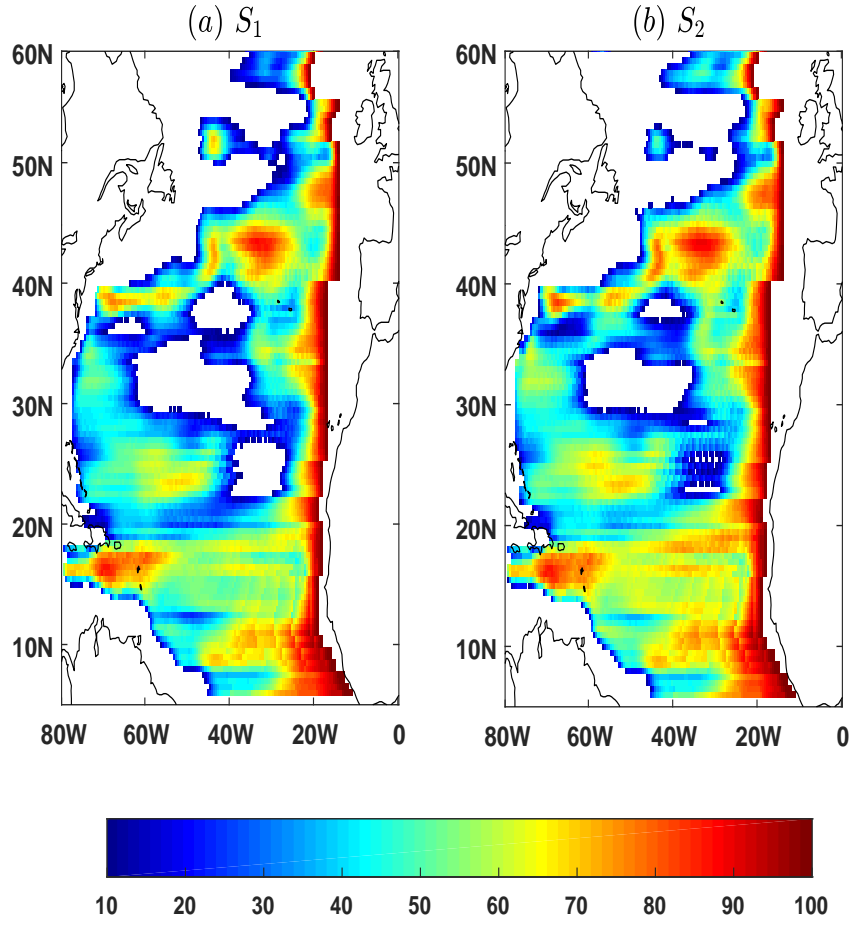


Fig. 2: (a) and (b) show forecast skill when $F_Q = 0$ and $F_Q \neq 0$ in Eq. (6)